NEW OPPORTUNITIES FOR THE MICROSTRUCTURAL ANALYSIS OF WOOD FIBRE NETWORKS

Thomas Walther[1], Heiko Thoemen[1], Kasim Terzic[2], Hans Meine[2]

[1]*University of Hamburg, Department of Wood Science, Leuschnerstrasse 91, 21031 Hamburg, Germany, t.walther@holz.uni-hamburg.de*
[2]*University of Hamburg, Department of Informatics, Vogt-Koelln-Strasse 30, 22527 Hamburg, Germany, terzic@informatik.uni-hamburg.de*

SUMMARY

3D image data sets of microtomography data from medium density fibreboard (MDF) have been analyzed using image analysis routines adapted to the material structure. The samples examined in this study covered a density range from 300 kg/m^3 to 1000 kg/m^3. Fibre orientation, fibre surfaces, contact areas and the volume covered by cell wall material, intra-fibre lumen and inter-fibre voids were analyzed and a simulation of the permeability and thermal conductivity was performed on small sub volumes of the data sets. The analysis of the microstructure will help us to better understand the fundamental mechanisms affecting the mechanical and physical properties of wood fibre based composites. Such understanding is essential if we want to optimize the performance of existing wood-based panels or to design innovative materials.

INTRODUCTION

The production of medium density fibreboard (MDF) and high density fibreboard (HDF) in Europe reached the level of 12 million m^3 by the beginning of 2005. The future of this product is highly dependent on the effort to increase the performance under service conditions and to decrease production costs by optimizing the production process. One step to improve the board quality is to find out more about its structure. Fibreboards have been subject to different microstructural investigations during recent years (Jayne 1972, Murmanis et al. 1986a, 1986b, Butterfield et al. 1992; Shaler et al. 1998, Groom et al. 1999, Faessel et al. 2005). However, most of the work published before 1998 deals with microscopic approaches, providing only limited information about the complete 3D-structure of these boards. One way to close this gap is the use of microtomography (µCT) to gain 3D images of the wood fibre network and to quantitatively analyze its structure. Investigations on the 3D-structure by Wang and Shaler (1998), Shaler et al. (1998), Groom et al. (1999), Faessel et al. (2005) and Lux et al. (2006a, 2006b) gave new insights in the structure of the fibre network. However, a comprehensive quantitative analysis of the microstructure has not been reported yet. This research work deals with a highly automated analysis of microtomography images regarding the identification of single fibres, fibre bundles, fibre orientation and the calculation of the contact areas and inner and outer surface of boards with different densities. Included in this approach is the simulation of the permeability and thermal conductivity on the basis of 3D data.

MATERIALS AND METHODS

Sample preparation

Different laboratory MDF samples made from commercial fibreboard furnish consisting of softwood fibres (*Pinus sylvestris*) have been prepared. The fibres were treated with an urea formaldehyde adhesive (BASF Kaurit 350 UF-resin) in a drum blender resulting in a total resin content of 10 % solid resin related to the dry weight of the board. Laboratory MDF samples with a thickness of 5 mm and a diameter of 100 mm with target densities ranging from 300 kg/m^3 to 1000 kg/m^3 were produced using the computer-controlled miniature hot-

pressing system IPATES (Integrated Pressing And Testing System). The pressing program consisted of a 5 s closing step until the target thickness of 5 mm was reached and a strain holding stage of 75 s plus an opening stage of 10 s to release the internal gas pressure. Afterwards, the density profiles of the laboratory MDF were examined using a Rayscan density scanner and samples for microtomography investigations with a size of 2 x 2 x 5 mm were cut out. The cutting surfaces were smoothed using razorblades to gain square samples.

Microtomography

The samples were scanned using synchrotron radiation based X-ray microtomography (SRμCT) at the Hamburger Synchrotonstrahlungslabor of the Deutsches Elektronen Synchroton (HASYLAB at DESY) in Hamburg, Germany. SRμCT has a few advantages compared to conventional microfocus X-ray microtomography systems, e.g. a monochromatic parallel beam with an adjustable photon energy that can be modified to examine materials of different structure and size (Bernhardt et al. 2004). Known effects of microfocus μCT systems due to a cone beam and a low intensity X-ray source, e.g. beam hardening effects and huge artefacts, limit the use of these systems for fibreboard structures.

The measurements of the MDF samples were carried out using the SRμCT equipment developed by the GKSS Research Centre at HASYLAB beamline BW2 at a photon energy of 12 keV to match the low absorption of the wood fibres. The magnification was set to 3.98 resulting in an effective pixel size of 2.28 μm.

Each sample was scanned at projection angles from 0° to 180° in steps of 0.25° leading to 720 projections with a size of 1536 x 1024 pixels. The data were reconstructed to a stack of 2D images with a size of 1536 x 1536 pixels using a filtered-backprojection algorithm. For each sample, two scans were recorded so that a height of 4 mm from one to almost the other surface layer was available for the analysis. Due to the symmetrical density profile, a scan over the entire thickness of the sample was not necessary. The resulting 3D data set had a size of 1536 x 1536 x 2028 voxels (voxel = volumetric pixel) shown in Figure 1.

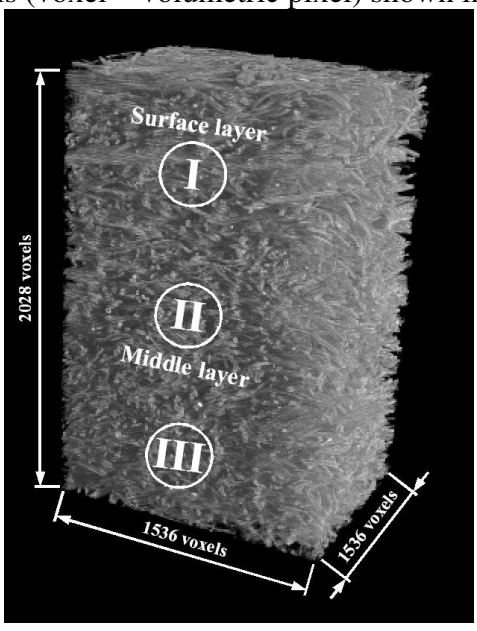

Figure 1: Reconstruced 3D-Volume of a MDF with a density of 300 kg/m^3. The side length of one voxel is 2.28 μm. The surface layer and the middle layer are marked. Areas of the chosen sub volumes (256^3 voxels, 512 x 512 x 256 voxels respectively) are numbered from I to III.

3D image analysis

At least, several sub volumes with a size of 256 x 256 x 256 voxels and 512 x 512 x 256 voxels were extracted from surface layer (named I in Figure 1) and intermediate layer positions (named II and III in Figure 1) from the 3D data sets of each sample for the image analysis. The size of the sub volumes was limited due to memory requirements and computer power because a complete 3D data set had a size of 4 GB.

The sub volumes were analyzed using the VIGRA image processing library, an open source library developed at the University of Hamburg (http://kogs-www.informatik.uni-hamburg.de/~koethe/vigra/) and C++. Image analysis algorithms were implemented in routines that were adjusted to the material structure. The flow chart in Figure 2 shows the steps of the segmentation and image analysis process to separate air regions and fibres.

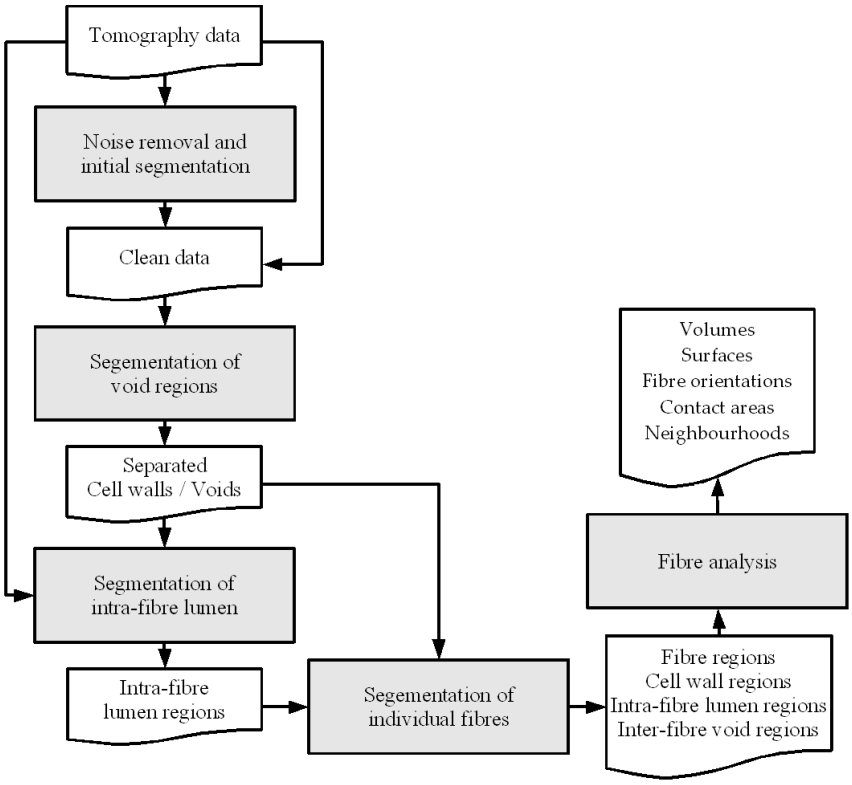

Figure 2: Flow chart for segmentation and image analysis of the selected sub volumes.

The first aim to evaluate the tomography data was a segmentation into cell wall material, intra-fibre lumen and inter-fibre voids. For this purpose, noise and systematic errors from the reconstruction had to be removed, and then the void regions had to be identified and separated from the cell wall material. After this, a separation between enclosed air inside a fibre, the so-called intra-fibre lumen, and air outside of the fibres, the so-called inter-fibre voids, was performed. The segmentation led to the identification of individual fibres that were later to be analyzed regarding their volume, orientation, inner and outer surface, contact areas and neighbouring fibres, above fibre bundles could be detected.

Simulation of mat permeability and thermal conductivity

The tomography data were also suitable to simulate gas permeability and thermal conductivity of the fibre mats for different density levels, and to compare the simulation results with own experimental data. Sub volumes with a size of 256^3 voxels or 512 x 512 x 256 voxels respectively, of the MDF data sets from 300 to 1000 kg/m^3 were selected for the simulation of the mat permeability and thermal conductivity at the Fraunhofer Institut für Techno- und

Wirtschaftsmathematik (ITWM) in Kaiserslautern, Germany. The Department of Flow and Complex Structures of the ITWM has developed a series of software tools for the calculation of the permeability and the thermal conductivity of porous materials. The use of 3D data from µCT sources allows the modelling and simulation of multiaxial flow processes in complex structures.

RESULTS AND DISCUSSION

Microtomography

3D renderings of reconstructed sample volume data sets are shown in Figure 3. It can be seen that the packing of the fibres increases with increasing density until single fibres become less and less visible and the space between the fibres, identified and named in this context as inter-fibre voids, is decreasing leaving only a few voids in the structure.

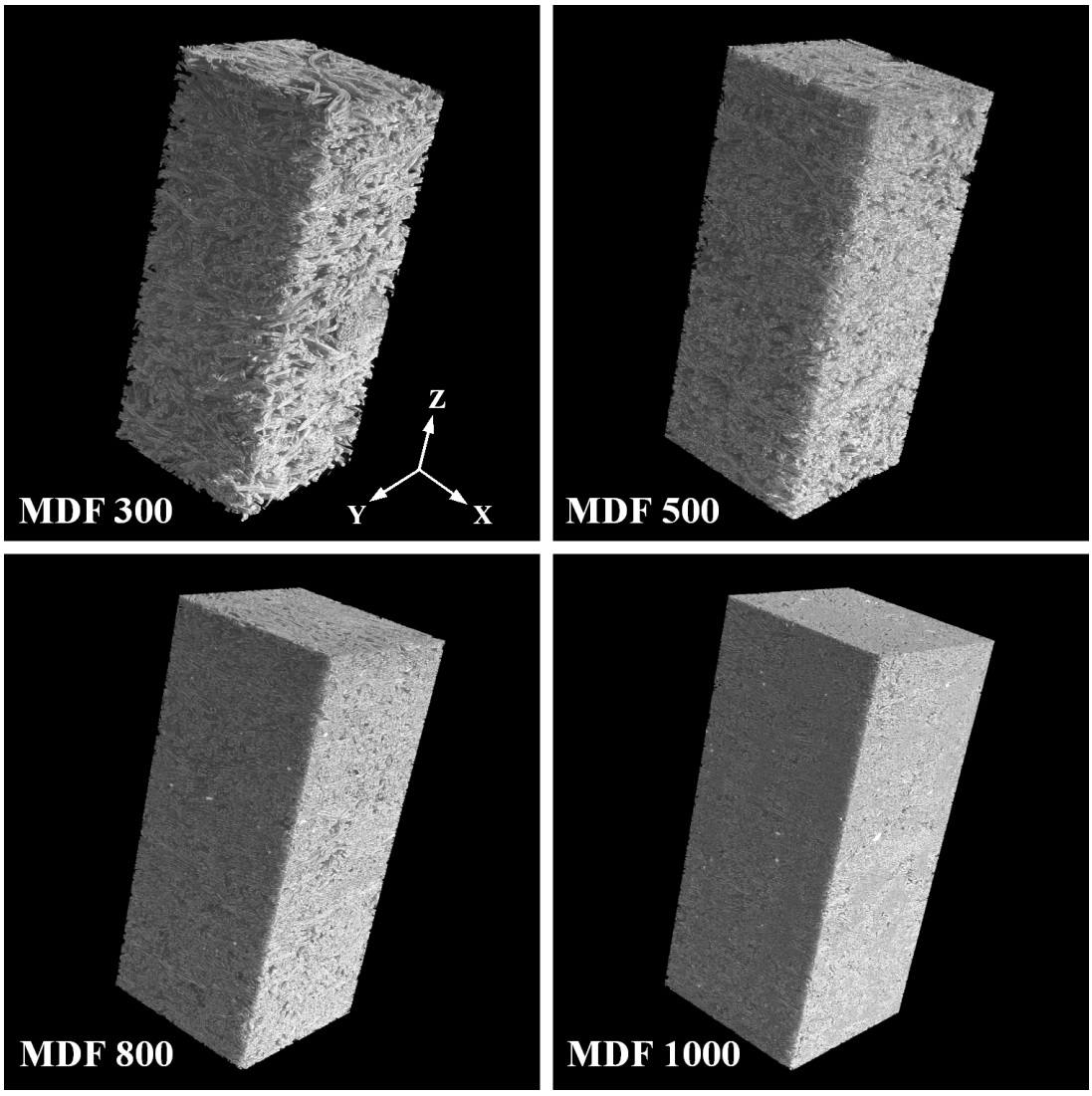

Figure 3: Four 3D volume renderings of the scanned laboratory MDF samples showing the area close to the middle layer with an average density close to the target density of 300, 500, 800 and 1000 kg/m^3. The edge length of the square blocks in X- and Y-direction is 1 mm and 2.3 mm in Z-direction.

Figure 4 shows virtual 2D slices in YZ-direction through intermediate layer sections of the MDF samples with target densities from 300 to 1000 kg/m3. The dense packing of fibres is

apparent for the MDF 800 and MDF 1000 samples, but the insufficient resolution becomes the limiting factor to identify individual fibres of the highly densified areas. Nevertheless, earlywood fibres and latewood fibres can be distinguished in the MDF 300 and MDF 500 samples and the presence of fibre bundles mainly consisting of earlywood fibres, e.g. in the upper left corner of the MDF 300 sample, is evident.

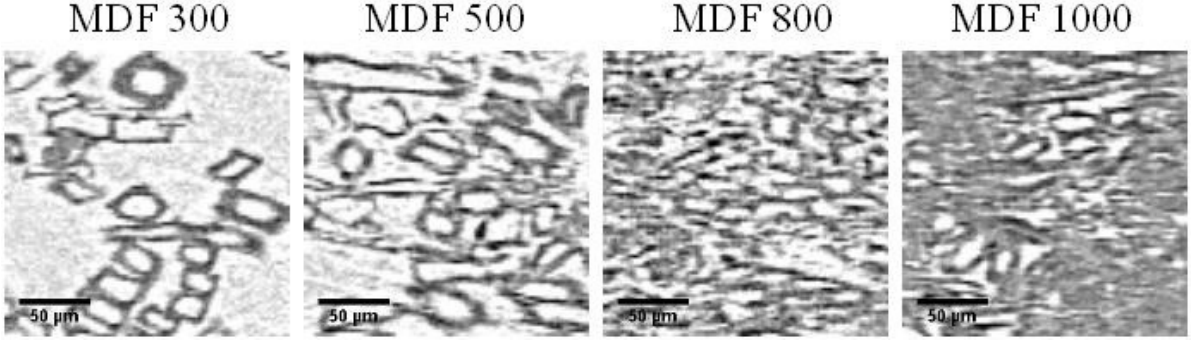

Figure 4: Virtual 2D YZ-slice through a 200 x 200 µm area of MDF samples with target densities from 300 to 1000 kg/m^3 from intermediate layer sections. The increasing densification of the fibres and the limit of the resolution of 2.28 µm in the highly densified samples are apparent.

3D image analysis

The 3D image analysis consisted of the successful segmentation of the cell wall material, fibre lumen and the outer air using the selected sub-volumes. Individual fibres have been identified and labelled. A sample of a MDF 300 sub volume with individually marked fibres is shown Figure 5.

Figure 5: Individually labelled fibres using a system of six different colours of a MDF 300 sub-volume. The edge length of the displayed cube is 588 µm.

The voxels belonging to one of the three classes were counted for all sub volumes and the results are displayed in Figure 6. It has to be noted that the density of the samples displayed on the X-axis was calculated on the basis of the segmented cell wall material with each voxel having a density of 1500 kg/m^3 as the estimated density of pure cell wall material. The calculated densities of the sub volumes compared to the real density of the samples measured by the Rayscan density scanner increased by this calculation up to 25%, due to an unavoidable

overestimation of the cell wall material during the segmentation procedure. In other words, the average thickness of the cell walls was increased up to 25% through segmentation. However, this error has a minor effect on the results of this analysis only, as the calculated densities instead of the real densities were used for the simulation of the permeability and thermal conductivity; for evaluating other parameters such as the fibre orientation the real densities were used.

Figure 6 indicates that the fibre lumen decreases non-linearly after reaching a density of 1100 kg/m^3. The collapse of latewood fibre cell walls at a certain pressure might be responsible for this effect. Both, the curves for inter-fibre voids and intra-fibre lumen in Figure 6 show a nearly linear trend up to a sample density of 1100 kg/m³; while the inter-fibre voids decrease, the fraction of the intra-fibre lumen increases. Obviously, compressing the fibre mat at low and intermediate density levels causes the inter-fibre voids to diminish, but not the intra-fibre lumen. Only above 1100 kg/m³ the latewood fibres start to collapse, bringing the fraction of the intra-fibre lumen back to zero at a sample density of 1500 kg/m³. The fraction of the inter-fibre voids already reaches zero at 1300 kg/m³. Above this density, all voids inside the fibre mat can be allocated to the intra-fibre lumen. Clearly, gas flow through the mat at such high densities is not possible anymore which was shown in the next paragraph called simulation.

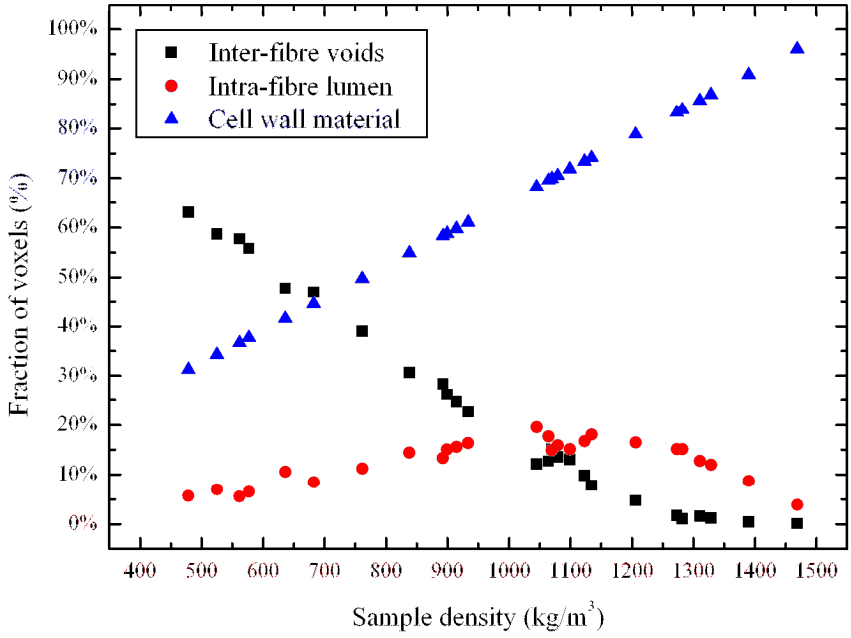

Figure 6: Fraction of voxels identified as cell wall material, intra-fibre lumen and inter-fibre voids.

Another interesting result is the free fibre surface in contact with the inter-fibre voids and the intra-fibre lumen shown in Figure 7. The contact area was calculated using a marching cube algorithm that gives a more accurate value of the surface area than a sum of voxels in contact with inter-fibre voids. A maximum value for the contact area with the inter-fibre voids was reached at a density of 700 to 750 kg/m^3. The maximum for the values for the inner surface of the fibres can be found at a density of about 1100 kg/m^3 which is similar to the density found in Figure 6 when the cell wall starts to collapse and the lumen volume is reduced.

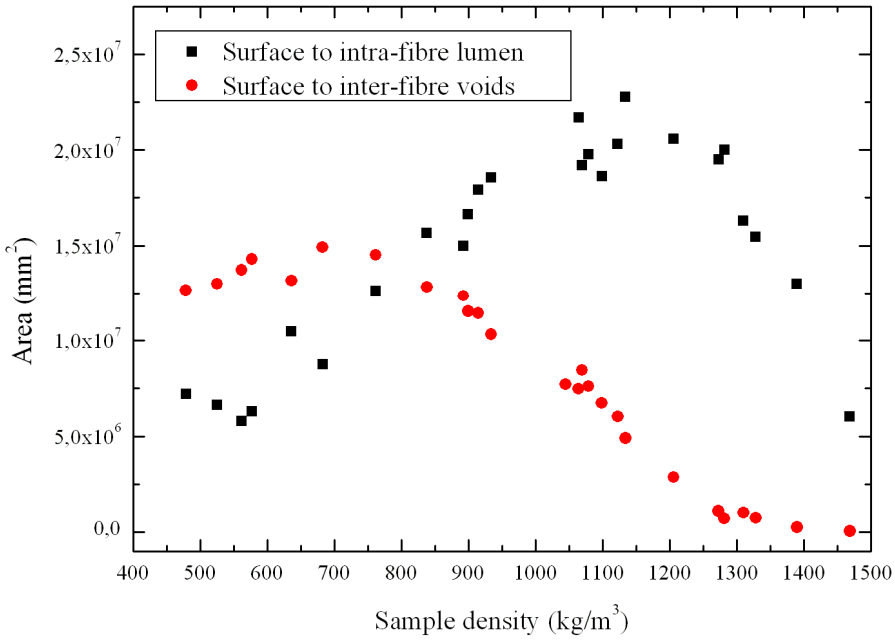

Figure 7: Calculated surface area in µm² for the fibre surfaces in contact with outer air and lumen for a density range from 450 to 1470 kg/m³.

The fibre orientation for each fibre in the sub volumes was calculated and evaluated. It was found that a random distribution in X- and Y-direction was apparent and that the orientation in Z-direction was insignificant for all density levels. It can be concluded that the fibres are already completely oriented in the XY-plane at a density of 300 kg/m³. An analysis of the contact areas between the fibres was helpful to find fibre bundles that consist of a few single fibres that share a large border. The average contact areas of about 90 µm² between two fibres were nearly similar for all densities with large deviations due to the existence of fibre bundles and single fibres in more or less parallel orientation. Future research will focus on this phenomenon for MDF.

Simulation

Results of the simulation of the permeability and thermal conductivity are displayed in Figure 8 and Figure 9. Figure 8 shows the results of the permeability calculation in Z-direction on six sub volumes chosen out of area I and II (marked in Figure 1) of the MDF 300, MDF 500 and MDF 800 3D data sets. The curve represents the formula for the permeability found by experiments for the same fibreboard furnish used for the µCT analysis. Please note that the density values of the samples were up to 25% higher than the target densities, as already described above.

The simulation results and the experimental values fit well, although the simulated permeability of the lower density samples seems to be somewhat overestimated. The permeability of the MDF 1000 samples (actual densities around 1450 kg/m³, not displayed in Figure 8) tends to zero, as it was expected. There are no pathways left for gas flow within the highly consolidated mat (see also Figure 6).

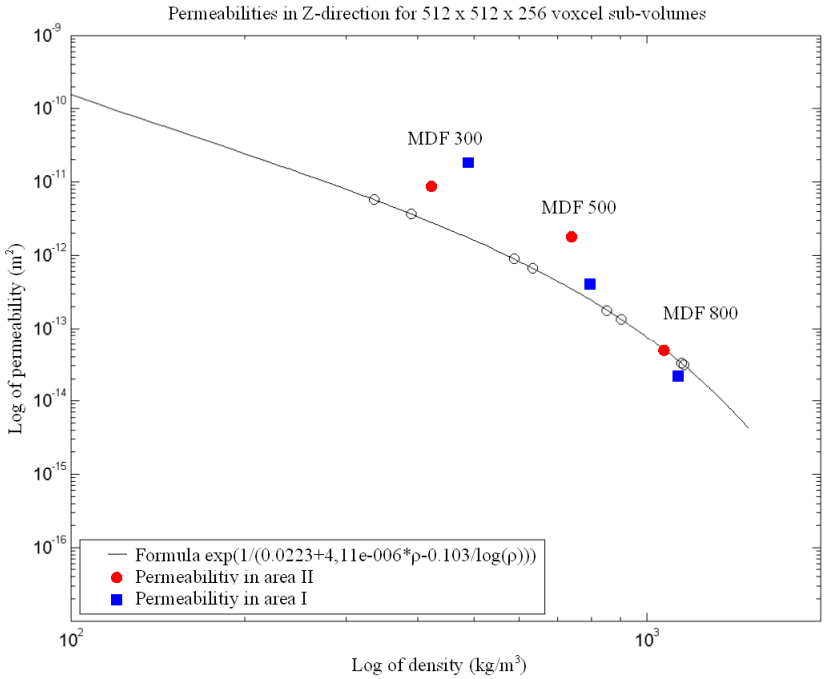

Figure 8: Permeability in Z direction for the 512 x 512 x 256 voxel sub volumes. The calculated permeability for MDF 1000 tended to be zero.

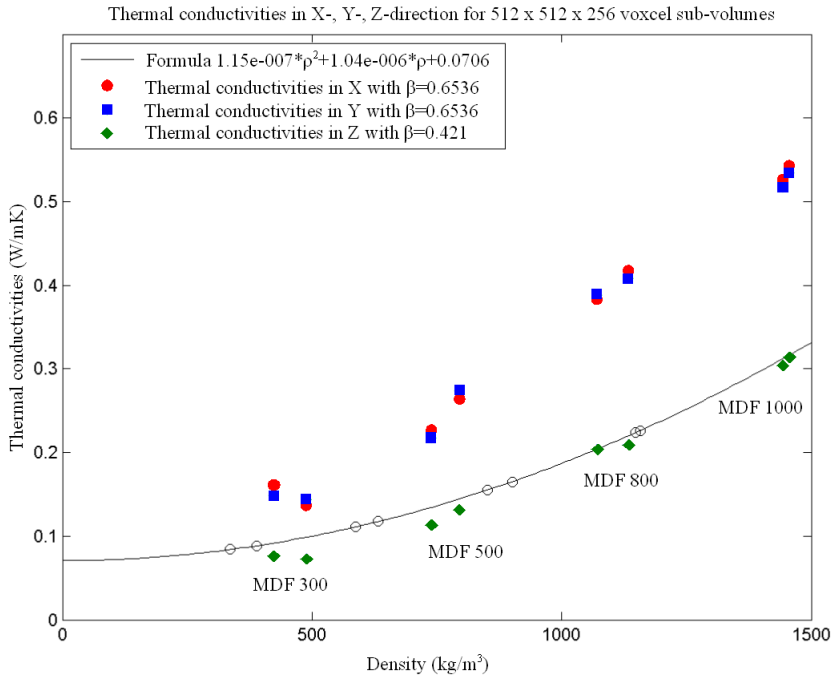

Figure 9: Thermal conductivity in X, Y and Z direction for the 512 x 512 x 256 voxel sub volumes.

In Figure 9, the simulated thermal conductivity of the fibreboard furnish is displayed for the X-, Y- and Z-direction. Thermal conductivity values for the cell wall material were taken from Maku (1954) in Kollmann and Malmquist (1956), with $\beta = 0.421$ W/(mK) perpendicular to the fibre axis and $\beta = 0.654$ W/(mK) in fibre direction. In addition, a curve fitted to cross-

sectional thermal conductivity values measured for the same fibreboard furnish as was used for the microtomography analysis is displayed.
The simulated thermal conductivity corresponds very well with the experimental data over the entire density range. For the thermal conductivity in X- and Y-direction neither own measurements have been conducted, nor have such data been reported in the literature, so far. Apparently, the values presented in Figure 9 are the first reliable data of the thermal conductivity within the plane of a randomly orientated mat. The results for the 256^3 voxel sub volumes were similar to the 512 x 512 x 256 voxel sub volumes indicating that the size of the sub volumes should be representative for a certain layer of the mat. Further research is planned to validate the results with theoretical models.

CONCLUSIONS

Microtomography combined with powerful image analysis tools offers a large variety of methods to analyse fibreboard structures. Additionally, it supplements standard microscopy techniques by allowing insights in the structure and the opportunity to conduct virtual cuts through the sample in any direction. The analysis of the unchanged and undamaged 3D structure of MDF at different density levels offers the opportunity to enhance the production quality by changing the fibre orientation and to simulate the production process. Another possibility might exist to optimize the resin distribution on the fibres by visualizing the resin distribution with suitable staining substances which is subject to further research.
Nevertheless, the algorithms and routines used for image analysis had to be adapted to the fibreboard structure which requires comprehensive knowledge about the morphology of the fibres and image analysis systems.

ACKNOWLEDGEMENT

The authors gratefully acknowledge the financial support of the Arthur and Aenne Feindt Foundation (Hamburg), Felix Beckmann, Tilman Donath and Jens Fischer from the GKSS Research Centre at DESY (Hamburg) and Volume Graphics GmbH (Heidelberg) for their technical support.

REFERENCES

BERNHARDT R, SCHARNWEBER D, MÜLLER B, THURNER P, SCHLIEPHAKE H, WYSS P, BECKMANN F, GOEBBELS J, WORCH H (2004): Comparison of microfocus- and synchrotron x-ray tomography for the analysis of osteointegration around Ti6Al4V-Implants: European Cells and Materials Journal **7**: 42-51

BUTTERFIELD B, CHAPMAN K, CHRISTIE L, DICKSON A (1992): Ultrastructural characteristics of failure surfaces in medium density fibreboard: Forest Products Journal **42** (6): 55-60

FAESSEL M, DELISÉE C, BOS F, CASTÉRA P (2005): 3D modelling of random cellulosic fibrous networks based on X-ray tomography and image analysis: Composites Science and Technology **65** (13): 1931-1940

GROOM L, MOTT L, SHALER S M (1999): Relationship between Fiber Furnish Properties and the Structural Performance of MDF: Proceedings of the 33rd International Particleboard/Composite Materials Symposium , Washington State University, Pullman, Washington, USA, 13th-15th April 1999: 89-100

JAYNE B A (1972): Theory and Design of Wood and Fiber Composite Materials: Syracuse University Press, New York, USA: 219-253

KOLLMANN F, MALMQUIST L (1956): Über die Wärmeleitzahl von Holz und Holzwerkstoffen: Holz als Roh- und Werkstoff **14** (6): 201-204

LUX J, DELISÉE C, THIBAULT X (2006a): 3D characterization of wood based fibrous materials: an application: Image Analysis & Stereology **25**: 25-35

LUX J, AHMADI A, GOBBÉ C, DELISÉE C (2006b): Macroscopic thermal properties of real fibrous materials: Volume averaging method and 3D image analysis: International Journal of Heat and Mass Transfer **49** (11-12): 1958-1973

MAKU T (1954): Studies on the heat conduction in wood: Wood Research Bulletin **13**: 1-80. Kyoto Unversity, Japan

MURMANIS L, MYERS G C, YOUNGQUIST J (1986a): Fluorescence microscopy of hardboards: Wood and Fiber Science **18** (2): 212-219

MURMANIS L, YOUNGQUIST J A, MYERS G C (1986b): Electron microscopy study on hardboards: Wood and Fiber Science **18** (3): 369-375

SHALER S M, KEANE D, WANG H, MOTT L, LANDIS E, HOLZMAN L (1998): Microtomography of cellulosic structures: TAPPI Proceedings of Product and Process Quality Conference, Milwaukee, Wisconsin, USA, 18th-23rd October 1998: 89-96

WANG H, SHALER S M (1998): Computer-Simulated Three-Dimensional Microstructure of Wood Fibre Composite Materials: Journal of Pulp and Paper Science **24** (10): 314-319